American Mineralogist, Volume 89, pages 976–980, 2004

Hydrothermal synthesis and crystal chemistry of the new strontium uranyl selenites, $Sr[(UO_2)_3(SeO_3)_2O_2]\cdot 4H_2O$ and $Sr[UO_2(SeO_3)_2]$

PHILIP M. ALMOND AND THOMAS E. ALBRECHT-SCHMITT*

Department of Chemistry, Auburn University, Auburn, Alabama 36849, U.S.A.

ABSTRACT

The reaction of UO_3 with SeO_2 in the presence of $SrCl_2\cdot 6H_2O$ and $Sr(OH)_2\cdot 8H_2O$ in supercritical water at 425 °C for 3 d results in the formation of the new strontium uranyl selenites, $Sr[(UO_2)_3(SeO_3)_2O_2]\cdot 4H_2O$ (1) and $Sr[UO_2(SeO_3)_2]$ (2). The single crystal X-ray structures of type 1 and type 2 were solved by direct methods and refined by full-matrix least-squares methods. Crystallographic data (193 K): (1), monoclinic, space group $C2/m$, a = 17.014(2), b = 7.0637(7), and c = 7.1084(7) Å, β = 100.544(2)°, Z = 2, $R(F)$ = 0.0361 for 79 parameters with 1132 reflections with $I > 2\sigma(I)$, wR_2 = 0.0998 for all data; (2), triclinic, space group $P\bar{1}$, a = 5.6722(4), b = 6.7627(5), and c = 11.2622(8) Å, α = 104.698(1)°, β = 93.708(1)°, γ = 109.489(1)°, Z = 2, $R(F)$ = 0.0373 for 110 parameters with 1902 reflections with $I > 2\sigma(I)$, wR_2 = 0.0856 for all data. The structure of type 1 contains two-dimensional $^2_\infty[(UO_2)_3(SeO_3)_2O_2]^{2-}$ sheets with the same topology as those found in guilleminite, $Ba[(UO_2)_3(SeO_3)_2O_2]\cdot 3H_2O$, and marthozite, $Cu[(UO_2)_3(SeO_3)_2O_2](H_2O)_8$. Sr^{2+} cations and H_2O groups occur between the layers. In contrast, the structure of type 2 contains one-dimensional $^1_\infty[UO_2(SeO_3)_2]^{2-}$ ribbons with Sr^{2+} cations residing between them. This compound is isostructural with its Ca^{2+}-containing analog.

INTRODUCTION

Uranyl minerals containing the selenite anion, SeO_3^{2-}, are rare, but include in the following: derriksite, $Cu_4[UO_2(SeO_3)_2](OH)_6$ (Ginderow and Cesbron 1983a), demesmaekerite, $Pb_2Cu_5[UO_2(SeO_3)_3]_2(OH)_6(H_2O)_2$ (Ginderow and Cesbron 1983b), guilleminite, $Ba[(UO_2)_3(SeO_3)_2O_2](H_2O)_3$ (Cooper and Hawthorne 1995), and marthozite, $Cu[(UO_2)_3(SeO_3)_2O_2](H_2O)_8$ (Cooper and Hawthorne 2001). Piretite, $Ca[(UO_2)_3(SeO_3)_2(OH)_4]\cdot 4H_2O$, is also reported to contain the selenite anion, but its crystal structure is unknown (Vochten et al. 1996). The majority of uranyl compounds, both naturally occurring and synthetic, are layered (Burns et al. 1996). This is a direct consequence of uranyl-containing polyhedra typically condensing perpendicular to the terminal, trans dioxo, $(O=U=O)^{2+}$, unit (Burns et al. 1996). These polyhedra take the form of UO_6 tetragonal bipyramids, UO_7 pentagonal bipyramids, and UO_8 hexagonal bipyramids, with UO_7 polyhedra being found in most phases (Burns et al. 1996). Derriksite and demesmaekerite show a departure from typical layered uranyl topologies by forming one-dimensional chains of UO_6 tetragonal bipyramids or UO_7 pentagonal bipyramids bridged by selenite anions. This dimensional reduction can be ascribed to the stereochemically active lone-pair of electrons at the Se^{4+} centers (Almond et al. 2002). Guilleminite and marthozite both contain topologically identical $^2_\infty[(UO_2)_3(SeO_3)_2O_2]^{2-}$ sheets that are formed from chains of edge-sharing UO_7 pentagonal bipyramids and UO_8 hexagonal bipyramids that are bridged by SeO_3^{2-} anions (Burns et al. 1996; Cooper and Hawthorne 1995; Cooper and Hawthorne 2001). This sheet topology is based on that of phosphuranylite, $KCa(H_2O)_3(UO_2)[(UO_2)_3(PO_4)_2O_2]_2\cdot 8H_2O$ (Demartin et al. 1991). It is interesting to note that the carbonate anion can play the same role as that of selenite in uranyl phases, for example, in the sheet topology of fontanite, $Ca[(UO_2)_3(CO_3)_2O_2]\cdot 6H_2O$, which is also based on that of phosphuranylite (Hughes and Burns 2003).

Synthetic uranyl selenites are a rapidly growing group of compounds that include $UO_2(SeO_3)$ (Loopstra and Brandenburg 1978), $UO_2(HSeO_3)_2\cdot H_2O$ (Mistryukov and Michailov 1983), $[NH_4]_2[UO_2(SeO_3)_2]\cdot 0.5H_2O$ (Koskenlinna et al. 1997), $A[UO_2(HSeO_3)(SeO_3)]$ (A = NH_4, K, Rb, Cs, Tl) (Koskenlinna and Valkonen 1996; Almond and Albrecht-Schmitt 2002), $Ag_2UO_2(SeO_3)_2$ (Almond and Albrecht-Schmitt 2002), $PbUO_2(SeO_3)_2$ (Almond and Albrecht-Schmitt 2002), $AE[UO_2(SeO_3)_2]$ (AE = Ca, Ba) (Almond et al. 2002), $Sr[UO_2(SeO_3)_2]\cdot 2H_2O$ (Almond et al. 2002), $[C_4H_{12}N_2]_{0.5}[UO_2(HSeO_3)(SeO_3)]$ (Almond and Albrecht-Schmitt 2003), and $[C_6H_{14}N_2]_{0.5}[UO_2(HSeO_3)(SeO_3)]\cdot 0.5H_2O\cdot 0.5CH_3CO_2H$ (Almond and Albrecht-Schmitt 2003). The majority of these compounds contain two-dimensional uranyl sheet topologies constructed from UO_7 pentagonal bipyramids bridged by selenite anions that were originally recognized in $NH_4[UO_2(HSeO_3)(SeO_3)]$ (Koskenlinna and Valkonen 1996). $Ca[UO_2(SeO_3)_2]$ and $Sr[UO_2(SeO_3)_2]\cdot 2H_2O$ contain these same building units but instead are found to form complex one-dimensional uranyl selenite chains (Almond et al. 2002).

In an effort to understand the role of temperature and pressure in the formation of uranyl selenites, we have begun to explore the synthesis of these compounds in supercritical water. Our initial studies have resulted in the isolation of two-dimensional $Sr[(UO_2)_3(SeO_3)_2O_2]\cdot 4H_2O$ (type 1) and one-dimensional $Sr[UO_2(SeO_3)_2]$ (type 2). Herein we disclose the synthesis and crystal chemistry of these compounds.

* E-mail: albreth@auburn.edu

EXPERIMENTAL METHODS

Syntheses

UO_3 (99.8%, Alfa-Aesar), SeO_2 (99.4%, Alfa-Aesar), $SrCl_2·6H_2O$ (99.0%, Alfa-Aesar), and $Sr(OH)_2·8H_2O$ (99.999%, Alfa-Aesar) were used as received. Distilled 18 MΩ millipore water was used in these reactions. Infrared spectra were collected with a Nicolet 5PC FTIR spectrometer using KBr pellets.

For the synthesis of $Sr[(UO_2)_3(SeO_3)_2O_2]·4H_2O$ (1) and $Sr[UO_2(SeO_3)_2]$ (2) UO_3 (180 mg, 0.63 mmol), SeO_2 (101 mg, 0.91 mmol), $SrCl_2·6H_2O$ (75 mg, 0.28 mmol), and $Sr(OH)_2·8H_2O$ (130 mg, 0.49 mmol) were loaded in a quartz ampule followed by the addition of 0.5 mL of water (approx. 50% fill). The tube was frozen with liquid nitrogen, evacuated, sealed, and subsequently placed in a Leco-Tem-Press 27 mL autoclave filled with water. The autoclave was counter pressured with 2500 psi of argon and heated at a rate of 10 °C/min to 425 °C for 72 h, and then slow cooled at a rate of 0.2 °C/min. The tube was subsequently removed from the autoclave and frozen in liquid nitrogen to allow for safe opening. *Extreme caution should be taken when scoring and opening sealed tubes from supercritical reactions because these are typically under pressure*. The product consisted of a clear solution over yellow rods of type 1 and yellow prisms of type 2. The crystals were washed with methanol and allowed to dry. Manual separation of the crystals provided 109 mg (42% yield based on U) of type 1, and 164 mg (43% yield based on U) of 2. EDX analyses for $Sr[(UO_2)_3(SeO_3)_2O_2]·4H_2O$ and $Sr[UO_2(SeO_3)_2]$ provided a Sr:U:Se ratio of 1:3:2 and 1:1:2, respectively. The infrared results are as follows (values in cm^{-1}): (1) 909 ($\upsilon_{3[uranyl]}$, s), 865 ($\upsilon_{1[uranyl]}$, m), 839 (υ_{SeO_3} s, sh), 814 (υ_{SeO_3} m), 725 (υ_{SeO_3} m, br), 615 (υ_{SeO_3} s); (2) 912 ($\upsilon_{3[uranyl]}$ m, br), 866 ($\upsilon_{1[uranyl]}$ m), 839 (υ_{SeO_3} m), 821 (υ_{SeO_3} m, sh), 817 (υ_{SeO_3} m), 744 (υ_{SeO_3} s, sh), 725 (υ_{SeO_3} s, sh), 619 (υ_{SeO_3} m, br).

Crystallographic studies

Single crystals of (1) (0.046 × 0.012 × 0.010 mm) and (2) (0.049 × 0.025 × 0.015 mm) were mounted on glass fibers and aligned on a Bruker SMART APEX CCD X-ray diffractometer. For each crystal, intensity measurements were performed using graphite monochromated Mo*K*α radiation from a sealed tube and monocapillary collimator. SMART was used for preliminary determination of the cell constants and data collection control (Bruker 2000). The intensities of reflections of a sphere were collected by a combination of 3 sets of exposures (frames). Each set had a different φ angle for the crystal and each exposure covered a range of 0.3° in ω. A total of 1800 frames were collected with an exposure time per frame of 60 s for type 1 and 30 s for type 2.

For type 1 and type 2, determination of integrated intensities and global refinement were performed with the Bruker SAINT (v 6.02) software package using a narrow-frame integration algorithm. A face-indexed analytical absorption correction was initially applied using XPREP (Sheldrick 2001). Individual shells of unmerged data were corrected analytically and exported in the same format. These files were subsequently treated with a semiempirical absorption correction by SADABS (Sheldrick 2001). This provided final R_{int} values of 0.0385 and 0.0521 for type 1 and type 2, respectively. The program suite SHELXTL (v 6.12) was used for space group determination (XPREP), direct methods structure solution (XS), and least-squares refinement (XL) (Sheldrick 2001). The final refinements included anisotropic displacement parameters for all atoms and a secondary extinction parameter [0 for type 1 and 0.0026(5) for type 2]. There is evidence for minor stacking disorder in type 1 based on elongation of the thermal ellipsoids along **c**, which is perpendicular to the direction of sheet propagation. Similar stacking disorder has been recognized in other uranyl phases (Talley et al. 2000). Some crystallographic details are given in Table 1. Atomic coordinates and equivalent isotropic displacement parameters for $Sr[(UO_2)_3(SeO_3)_2O_2]·4H_2O$ (1) and $Sr[UO_2(SeO_3)_2]$ (2) are given in Tables 2 and 3, respectively. Anisotropic displacement parameters are given in Tables 4 and 5 for type 1 and type 2, respectively.

RESULTS AND DISCUSSION

Syntheses

It is well recognized in transition metal phosphate synthesis that a change from mild hydrothermal conditions (<250 °C, autogenously generated pressure) to supercritical conditions (>374 °C, up to 50 000 psi) often results in the formation of dramatically different products with a tendency toward forming denser phases at high temperature and pressure (Kolis and

TABLE 1. Crystallographic data for $Sr[(UO_2)_3(SeO_3)_2O_2]·4H_2O$ (1) and $Sr[UO_2(SeO_3)_2]$ (2)

Compound	(1)	(2)
Color and habit	Yellow rod	Yellow prism
Formula mass (amu)	1247.63	611.57
Space group	*C*2/*m* (No. 15)	$P\bar{1}$ (No. 2)
a (Å)	17.014(2)	5.6722(4)
b (Å)	7.0637(7)	6.7627(5)
c (Å)	7.1084(7)	11.2622(8)
α (°)	90	104.698(1)
β (°)	100.544(2)	93.708(1)
Γ (°)	90	109.489(1)
V (Å^3)	839.88(15)	388.61(5)
Z	2	2
T (°C)	–80	–80
λ (Å)	0.71073	0.71073
ρ_{calcd} (g cm^{-3})	4.933	5.226
μ(Mo*K*α) (cm^{-1})	364.11	370.44
$R(F)$ for $F_o^2 > 2\sigma(F_o^2)$*	0.0361	0.0373
$R_w(F_o^2)$†	0.0998	0.0856

* $R(F) = \Sigma \left\| F_o \right| - \left| F_c \right\| / \Sigma \left| F_o \right|$

† $R_w\left(F_o^2\right) = \left[\Sigma\left[w\left(F_o^2 - F_c^2\right)^2\right] / \Sigma\, wF_o^4\right]^{1/2}$; $w = 0.0543$ for 1 and 0.0326 for 2.

TABLE 2. Atomic coordinates and equivalent isotropic displacement parameters for $Sr[(UO_2)_3(SeO_3)_2O_2]·4H_2O$ (1)

Atom	*x*	*y*	*z*	U_{eq} (Å^2) *	Occupancy
U1	0	0	0	0.0091(2)	1
U2	–0.10866	1/2	0.95299	0.0095(2)	1
Sr1	0	–0.3221(3)	1/2	0.0095(2)	1/2
Se1	0.20653(7)	0	0.11359(19)	0.0111(3)	1
O1	0.1372(4)	0.1707(10)	0.0594(13)	0.031(2)	1
O2	0.2509(6)	0	0.9211(14)	0.024(2)	1
O3	0	–0.3158(14)	0	0.033(3)	1
O4	0.0007(6)	0	0.7440(16)	0.027(3)	1
O5	–0.1067(6)	1/2	0.2099(16)	0.027(3)	1
O6	–0.1110(6)	1/2	0.6961(14)	0.024(2)	1
O7	–0.1454(8)	–0.138(2)	0.433(2)	0.026(3)	1/2
O8	–0.2127(9)	–0.235(2)	0.470(2)	0.029(3)	1/2

* U_{eq} is defined as one-third of the trace of the orthogonalized U_{ij} tensor.

TABLE 3. Atomic coordinates and equivalent isotropic displacement parameters for $Sr[UO_2(SeO_3)_2]$ (2)

Atom	*x*	*y*	*z*	U_{eq} (Å^2) *
U1	0.16771(6)	0.25930(5)	0.16256(3)	0.00956(14)
Sr1	0.66515(16)	0.25268(13)	0.44132(8)	0.01025(19)
Se1	0.72939(17)	0.69349(14)	0.34103(8)	0.0104(2)
Se2	0.30283(17)	–0.19130(14)	0.12469(8)	0.0113(2)
O1	0.4421(11)	0.4831(9)	0.3429(6)	0.0112(13)
O2	0.9238(12)	0.6234(10)	0.4242(6)	0.0162(14)
O3	0.6827(13)	0.8965(10)	0.4413(6)	0.0165(14)
O4	0.3209(12)	0.0194(9)	0.2498(6)	0.0117(13)
O5	0.0974(13)	–0.1320(10)	0.0322(6)	0.0170(15)
O6	0.1163(13)	–0.4148(10)	0.1576(6)	0.0162(14)
O7	–0.0973(12)	0.1893(10)	0.2405(6)	0.0130(13)
O8	0.4347(12)	0.3326(11)	0.0898(6)	0.0143(14)

* U_{eq} is defined as one-third of the trace of the orthogonalized U_{ij} tensor.

TABLE 4. Anisotropic displacement parameters (Å^2 × 10^3) for $Sr[(UO_2)_3(SeO_3)_2O_2]·4H_2O$ (1)

Atom	U_{11}	U_{22}	U_{33}	U_{23}	U_{13}	U_{12}
U1	10(1)	5(1)	13(1)	0	3(1)	0
U2	9(1)	5(1)	15(1)	0	3(1)	0
Sr1	13(1)	6(1)	9(1)	0	1(1)	0
Se1	9(1)	7(1)	17(1)	0	3(1)	0
O1	15(4)	7(3)	66(6)	–11(3)	–6(3)	0(3)
O2	10(5)	49(7)	15(5)	0	3(4)	0
O3	10(5)	3(4)	84(9)	0	0(5)	0
O4	16(5)	46(7)	20(5)	0	5(4)	0
O5	9(5)	44(7)	27(6)	0	4(4)	0
O6	14(5)	45(7)	14(5)	0	4(4)	0
O7	17(7)	36(9)	21(7)	0(7)	-7(6)	15(7)
O8	37(8)	8(7)	40(9)	1(6)	4(7)	5(6)

Note: The anisotropic displacement factor exponent takes the form: $-2\pi^2[(ha^*)^2U_{11} + ... + 2hka^*b^*U_{12}]$.

TABLE 5. Anisotropic displacement parameters ($Å^2 \times 10^3$) for $Sr[UO_2(SeO_3)_2]$ (2)

Atom	U_{11}	U_{22}	U_{33}	U_{23}	U_{13}	U_{12}
U1	13(1)	8(1)	7(1)	2(1)	2(1)	3(1)
Sr1	11(1)	8(1)	11(1)	4(1)	2(1)	3(1)
Se1	12(1)	9(1)	11(1)	4(1)	3(1)	4(1)
Se2	16(1)	10(1)	10(1)	3(1)	3(1)	6(1)
O1	10(3)	6(3)	12(3)	−2(2)	2(2)	0(2)
O2	12(3)	14(3)	26(4)	12(3)	1(3)	4(3)
O3	18(4)	12(3)	19(4)	4(3)	6(3)	5(3)
O4	16(3)	7(3)	9(3)	−2(2)	0(2)	5(2)
O5	27(4)	11(3)	12(3)	4(3)	−5(3)	6(3)
O6	25(4)	11(3)	13(3)	3(3)	1(3)	9(3)
O7	12(3)	11(3)	12(3)	0(2)	2(2)	2(3)
O8	14(3)	18(3)	8(3)	0(3)	8(2)	4(3)

Note: The anisotropic displacement factor exponent takes the form: $-2\pi^2[(ha^*)^2U_{11} + ... + 2hka^*b^*U_{12}]$.

Korzenski 1999). We have applied this principle in our search for new uranyl selenite phases and found in some cases, such as in $UO_2(SeO_3)$ and $Ba[UO_2(SeO_3)_2]$, that some compounds can form under both mild and supercritical conditions. In contrast, in the presence of Sr^{2+}, UO_3 and SeO_2 react in aqueous media at 180 °C to form $Sr[UO_2(SeO_3)_2]\cdot 2H_2O$ (Almond et al. 2002). However, when the reaction temperature is increased to 425 °C, $Sr[(UO_2)_3(SeO_3)_2O_2]\cdot 4H_2O$ (1) and $Sr[UO_2(SeO_3)_2]$ (2) are observed to crystallize.

Structure descriptions

$Sr[(UO_2)_3(SeO_3)_2O_2]\cdot 4H_2O$ (1). The structure of type 1 is composed of UO_7 pentagonal bipyramidal units that share an edge to form a dimer. This dimer in turn shares two edges on each side with UO_8 hexagonal bipyramids creating one-dimensional chains that extend along **b**. These chains are then linked into two-dimensional $^2_\infty[(UO_2)_3(SeO_3)_2O_2]^{2-}$ sheets that extend in the **a-b** plane by bridging/chelating SeO_3^{2-} anions. A view of part of one of these sheets is shown in Figure 1. This sheet topology has been previously recognized in the minerals guilleminite, $Ba[(UO_2)_3(SeO_3)_2O_2](H_2O)_3$ (Cooper and Hawthorne 1995), and marthozite, $Cu[(UO_2)_3(SeO_3)_2O_2](H_2O)_8$ (Cooper and Hawthorne 2001). The guilleminite anionic sheet topology is related to the phosphuranylite topology, which includes both mineral and synthetic phases (Burns et al. 1996). In many of these phases the pyramidal selenite anion is replaced by tetrahedral anions where the fourth vertex remains terminal and occupies the same location as the stereochemically active lone-pair of electrons in the selenite anion. Several variants of this topology occur owing to the collective orientation of these bridging anions (Burns et al. 1996).

The two-dimensional $^2_\infty[(UO_2)_3(SeO_3)_2O_2]^{2-}$ sheets are connected to one another by Sr^{2+} cations and occluded water molecules. The Sr^{2+} cations, which reside in a half-occupied site, form long ionic contacts with both oxo atoms from the uranyl cations and with two water molecules forming a distorted dodecahedral geometry as shown in Figure 2. The Sr···O contacts range in distance from 2.757(13) to 2.860(7) Å. The water molecules lie between the layers and are disordered over two sites in a straightforward manner. A view of the structure along **c** showing the Sr^{2+} cations separating $^2_\infty[(UO_2)_3(SeO_3)_2O_2]^{2-}$ layers is shown in Figure 3.

The U = O bond distances in the uranyl cations are 1.819(10) and 1.821(11) Å in the UO_7 units, and 1.822(11) Å in the UO_8 polyhedra. The uranium atom of the UO_8 units resides at a 2/*m* site and is linear. The uranyl cation of the UO_7 units is approximately linear with a bond angle of 179.8(4)°. The U–O bond distances to the O atoms of the selenite anions as well as to the μ_3-oxo atom range from 2.235(6) to 2.374(7) Å in the UO_7 polyhedra and from 2.231(10) to 2.593(7) Å in the UO_8 groups. The bond valence sums for the U atoms are consistent with U^{6+} and are 6.08 and 5.81 for the UO_7 and UO_8 polyhedra, respectively. Parameters for seven- and eight-coordinate U^{6+} from Burns et al. (1997) were used these calculations. The Se-O bond distances are within normal limits and occur from 1.680(9) to 1.681(7) Å. The bond valence sum for Se1 is 4.26, and agrees reasonably well with Se^{4+} as expected (Brese and O'Keefe 1991). Selected bond distances are given in Table 6.

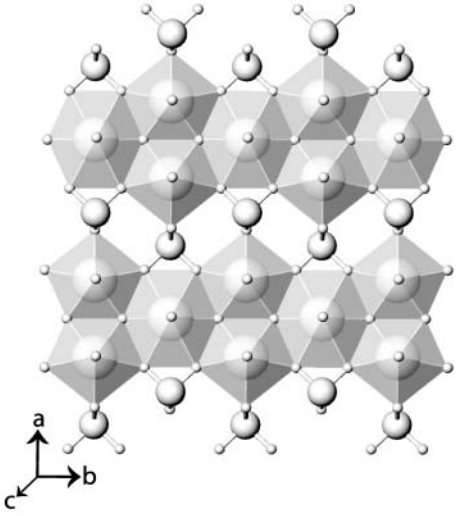

FIGURE 1. A view down **c** of the two-dimensional $^2_\infty[(UO_2)_3(SeO_3)_2O_2]^{2-}$ sheets that extend in the **ab** plane in $Sr[(UO_2)_3(SeO_3)_2O_2]\cdot 4H_2O$ (1).

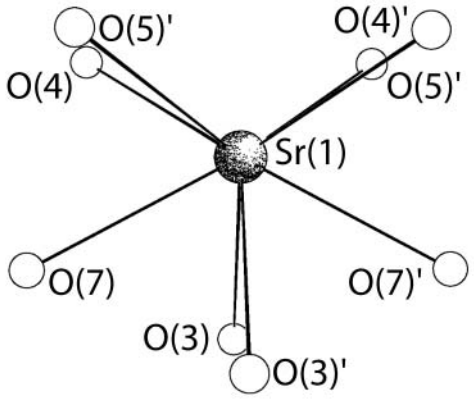

FIGURE 2. An illustration of the local Sr^{2+} cation environment showing a distorted dodecahedral geometry in $Sr[(UO_2)_3(SeO_3)_2O_2]\cdot 4H_2O$ (1).

$Sr[UO_2(SeO_3)_2]$ (2). Compound type 2 is isostructural with $Ca[UO_2(SeO_3)_2]$, which was previously synthesized under mild

hydrothermal conditions (Almond et al. 2002). Our discussion of the structure of this compound will therefore be brief. The structure of type 2 is built from one-dimensional $^{1}_{\infty}[UO_2(SeO_3)_2]^{2-}$ ribbons that propagate down **b**. These ribbons are obtained from pentagonal bipyramidal uranium centers that are bound by two terminal oxo groups, forming the uranyl moiety, and selenite anions that occur as monodentate and chelating/bridging groups. Part of one of these one-dimensional ribbons is depicted in Figure 4. The ribbons are joined to one another by Sr^{2+} cations that form long ionic contacts with surrounding O atoms ranging from 2.444(6) to 2.860(6) Å, creating a geometry that is best described as a distorted dodecahedron as illustrated in Figure 5. A packing diagram is shown in Figure 6.

The uranyl cation is approximately linear with a bond angle of 178.4(3)°. The U = O bond distances are 1.754(7) and 1.778(7) Å. The equatorial U-O bond distances display a range of values owing to the differing coordination modes of the selenite anion. These bond distances range from 2.302(6) to 2.562(6) Å. Using these bond distances, a bond valence sum of 5.99 was calculated for the uranium center in type 2. The Se-O bond distances range from 1.651(7) to 1.776(6) Å, and show differing lengths depending on whether they are bridging or terminal with terminal bonds being of shorter length. The bond valence sum for Se1 and Se2

TABLE 6. Selected bond distances (Å) for $Sr[(UO_2)_3(SeO_3)_2O_2]\cdot 4H_2O$ (1)

U1–O1	2.593(7)	U2–O1 (no. 6)	2.374(7)
U1–O1 (no. 1)	2.593(7)	U2–O2 (no. 5)	2.358(9)
U1–O1 (no. 2)	2.593(7)	U2–O3	2.235(6)
U1–O1 (no. 3)	2.593(7)	U2–O3 (no. 4)	2.235(6)
U1–O3	2.231(10)	U2–O5 (U = O)	1.821(11)
U1–O3 (no. 1)	2.231(10)	U2–O6 (U = O)	1.819(10)
U1–O4 (U = O)	1.822(11)	Se1–O1	1.681(7)
U1–O4′ (U = O)	1.822(11)	Se1–O1 (no. 2)	1.681(7)
U2–O1 (no. 1)	2.374(7)	Se1–O2	1.680(9)

Notes: No. 1 = –*x*, –*y*, –*z* + 2; no. 2 = *x*, –*y*, *z* ; no. 3 = –*x*, *y*, –*z* + 2; no. 4 = –*x*, -*y* – 1, –*z* + 2; no. 5 = *x* –– 1/2, *y* – 1/2, *z*; no. 6 = –*x*, *y* – 1, –*z* + 2.

TABLE 7. Selected bond distances (Å) for $Sr[UO_2(SeO_3)_2]$ (2)

U1–O1	2.302(6)	Se1–O1	1.776(6)
U1–O4	2.448(6)	Se1–O2	1.661(6)
U1–O5	2.359(6)	Se1–O3	1.651(7)
U1–O5 (no. 1)	2.562(6)	Se2–O4	1.700(6)
U1–O6 (no. 2)	2.331(6)	Se2–O5	1.723(6)
U1–O7 (U = O)	1.778(7)	Se2–O6	1.677(7)
U1–O8 (U = O)	1.754(7)		

Notes: No. 1 = *x*, *y* + 1, *z*; no. 2 = –*x*, –*y*, –*z*.

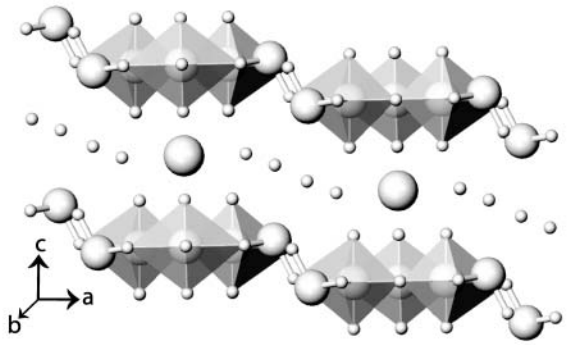

FIGURE 3. A depiction of part of the structure of $Sr[(UO_2)_3(SeO_3)_2O_2]\cdot 4H_2O$ (1) down **b** showing two-dimensional $^{2}_{\infty}[(UO_2)_3(SeO_3)_2O_2]^{2-}$ sheets separated from another by Sr^{2+} cations and water molecules.

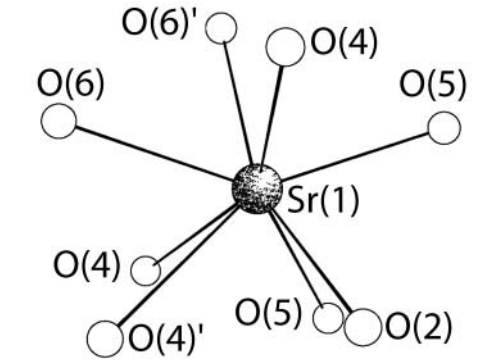

FIGURE 5. An illustration of the distorted dodecahedral environment around the Sr^{2+} cations in $Sr[UO_2(SeO_3)_2]$ (2).

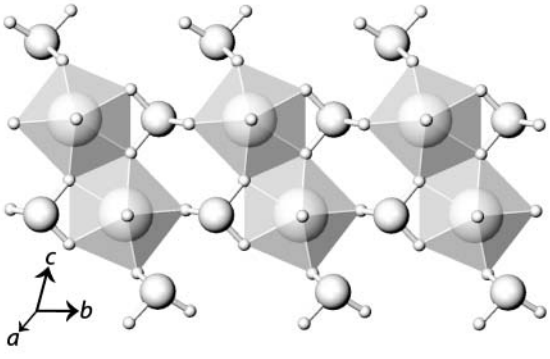

FIGURE 4. A view of one-dimensional $^{1}_{\infty}[UO_2(SeO_3)_2]^{2-}$ ribbons in $Sr[UO_2(SeO_3)_2]$ (2).

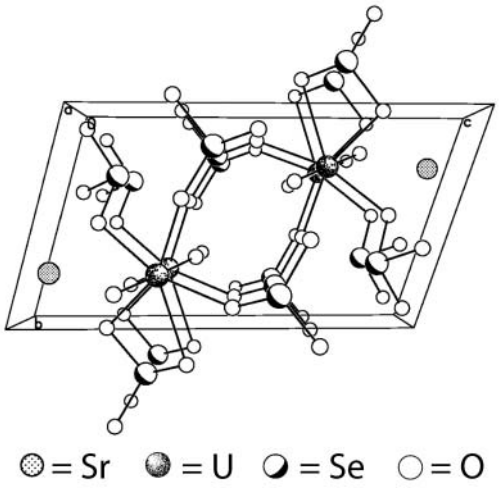

FIGURE 6. A drawing of the packing diagram of $Sr[UO_2(SeO_3)_2]$ (2) viewed down **a**.

are 4.14 and 4.06, respectively and are in good agreement with Se^{4+} (Brese and O'Keefe 1991). Selected bond distances are given in Table 7.

While the use of supercritical reaction conditions has yielded known anionic sheet and ribbon topologies in this present report, two key conclusions were reached during these studies. First, these conditions can give rise to the guilleminite anionic sheet topology, which has not previously been observed to form under ambient or mild hydrothermal conditions, even when appropriate cations are present (Almond et al. 2002). Second, whereas the reaction to form $Ca[UO_2(SeO_3)_2]$ required one month to reach completion (Almond et al. 2002), $Sr[UO_2(SeO_3)_2]$ could be isolated after a three day reaction. These results provide a strong indication that the use of supercritical conditions will allow for the synthesis of new uranyl selenite phases that do not form under milder conditions. These studies are currently underway.

ACKNOWLEDGMENTS

This research was sponsored by the Department of Energy, Heavy Elements Program (grant no. DE-FG02-01ER15187).

REFERENCES CITED

Almond, P.M. and Albrecht-Schmitt, T.E. (2002) Hydrothermal syntheses, structures, and properties of the new uranyl selenites $Ag_2(UO_2)(SeO_3)_2$, $M[(UO_2)(HSeO_3)(SeO_3)]$ (M = K, Rb, Cs, Tl), and $Pb(UO_2)(SeO_3)_2$. Inorganic Chemistry, 41, 1177–1183.

——— (2003) Do secondary and tertiary ammonium cations act as structure-directing agents in the formation of layered uranyl selenites? Inorganic Chemistry, 42, 5693–5698.

Almond, P.M., Peper, S.M., Bakker, E., and Albrecht-Schmitt, T.E. (2002) Variable dimensionality and new uranium oxide topologies in the alkaline-earth metal uranyl selenites $AE[(UO_2)(SeO_3)_2]$ (AE = Ca, Ba) and $Sr[(UO_2)(SeO_3)_2]\cdot 2H_2O$. Journal of Solid State Chemistry, 168, 358–366.

Brese, N.E. and O'Keefe, M. (1991) Bond-valence parameters for solids. Acta Crystallographica, B47, 192 197.

Bruker (2000) SMART (Version 5.611). Bruker AXS Inc., Madison, Wisconsin, U.S.A.

Burns, P.C., Miller, M.L., and Ewing, R.C. (1996) U^{6+} Minerals and inorganic phases: a comparison and hierarchy of crystal structures. Canadian Mineralogist, 34, 845–880.

Burns, P.C., Ewing, R.C., and Hawthorne, F.C. (1997) The crystal chemistry of hexavalent uranium: polyhedron geometries, bond-valence parameters, and polymerization of polyhedra. Canadian Mineralogist, 35, 1551–1570.

Cooper, M.A. and Hawthorne, F.C. (1995) The crystal structure of guilleminite, a hydrated Ba-U-Se sheet structure. Canadian Mineralogist, 33, 1103–1109.

——— (2001) Structure topology and hydrogen bonding in marthozite, $Cu^{2+}[(UO_2)_3(SeO_3)_2O_2](H_2O)_8$, a comparison with guilleminite, $Ba[(UO_2)_3(SeO_3)_2O_2](H_2O)_3$. Canadian Mineralogist, 39, 797–807.

Demartin, F., Diella, V., Donzelli, S., Gramaccioli, C.M., and Pilati, T. (1991) The importance of accurate crystal structure determination of uranium minerals. I. Phosphuranylite $KCa(H_2O)_3(UO_2)[(UO_2)_3(PO_4)_2O_2]_2\cdot 8H_2O$. Acta Crystallographica, B47, 439–446.

Ginderow, D. and Cesbron, F. (1983a) Structure de la derriksite, $Cu_4(UO_2)(SeO_3)_2(OH)_6$. Acta Crystallographica, C39, 1605–1607.

——— (1983b) Structure de la demesmaekerite, $Pb_2Cu_5(SeO_3)_6(UO_2)_2(OH)_6\cdot 2H_2O$. Acta Crystallographica, C39, 824–827.

Hughes, K.-A. and Burns, P.C. (2003) A new uranyl carbonate sheet in the crystal structure of fontanite, $Ca[(UO_2)_3(CO_3)_2O_2](H_2O)_6$. American Mineralogist, 88, 962–966.

Kolis, J.W. and Korzenski, M.B. (1999) Synthesis of inorganic solids. In P.G. Jessop and W. Leitner, Eds., Chemical Synthesis Using Supercritical Fluids, p. 213–241, Wiley, New York.

Koskenlinna, M. and Valkonen, J. (1996) Ammonium uranyl hydrogenselenite selenite. Acta Crystallographica, C52, 1857–1859.

Koskenlinna, M., Mutikainen, I., Leskelae, T., and Leskela, M. (1997) Low-temperature crystal structures and thermal decomposition of uranyl hydrogen selenite monohydrate, $UO_2(HSeO_3)_2\cdot H_2O$ and diammonium uranyl selenite hemihydrate, $(NH_4)_2UO_2(SeO_3)_2\cdot 0.5H_2O$. Acta Chemica Scandinavica, 51, 264–269.

Loopstra, B.O. and Brandenburg, N.P. (1978) Uranyl selenite and uranyl tellurite. Acta Crystallographica, B34, 1335–1337.

Mistryukov, V.E. and Michailov, Y.N. (1983) The characteristic properties of the structural function of the selenitogroup in the uranyl complex with neutral ligands. Koordinatsionnaya Khimiya, 9, 97–102.

Sheldrick, G.M. (2001a) SADABS 2001, Program for absorption correction using SMART CCD based on the method of Blessing: Blessing, R.H. (1995) An empirical correction for absorption anisotropy. Acta Crystallographica, A51, 33–38.

——— (2001b) SHELXTL, Version 6.12, An Integrated System for Solving, Refining, and Displaying Crystal Structures from Diffraction Data; Siemens Analytical X-ray Instruments, Inc. Madison, Wisconsin, 2001.

Talley, C.E., Gibbs, A.C., and Albrecht-Schmitt, T.E. (2000) Hydrothermal syntheses of layered uranium oxyfluorides: illustrations of dimensional reduction. Inorganic Chemistry, 39, 5174–5175.

Vochten, R., Blaton, N., Peeters, O., and Deliens, M. (1996) Piretite, $Ca(UO_2)_3(SeO_3)_2(OH)_4\cdot 4H_2O$, a new calcium uranyl selenite from Shinkolobwe, Shaba, Zaire. Canadian Mineralogist, 34, 1317–1322.

MANUSCRIPT RECEIVED SEPTEMBER 23, 2003
MANUSCRIPT ACCEPTED DECEMBER 7, 2003
MANUSCRIPT HANDLED BY LEE GROAT